Evidence of structural evolution in Sr_2RhO_4 studied by time-resolved optical reflectivity spectroscopy

Min-Cheol Lee,[1,2,3,*] Inho Kwak,[1,2] Choong H. Kim,[1,2] Bumjoo Lee,[1,2] Byung Cheol Park,[1,2] Junyoung Kwon,[1,2] Wonshik Kyung,[1,2] Changyoung Kim,[1,2] Tae Won Noh,[1,2] and Kyungwan Kim[4,†]

[1]*Center for Correlated Electron Systems (CCES), Institute for Basic Science (IBS), Seoul 08826, Republic of Korea*

[2]*Department of Physics and Astronomy, Seoul National University, Seoul 08826, Republic of Korea*

[3]*Center for Integrated Nanotechnologies, Los Alamos National Laboratory, Los Alamos, New Mexico 87545, USA*

[4]*Department of Physics, Chungbuk National University, Cheongju, Chungbuk 28644, Republic of Korea*

(Received 12 August 2019; revised manuscript received 2 December 2019; published 24 December 2019)

We investigate ultrafast dynamics from photoinduced reflectivity of Sr_2RhO_4 by using femtosecond near-infrared pulses. We observe a clear temperature dependent anomaly in its electronic dynamics which slows down below $T_S \sim 160$ K. In addition, coherent oscillations of the 5.3 THz A_{1g} phonon exhibit a 90° shift in its initial phase across T_S, indicating a structural change in octahedral rotation distortions. We propose that octahedral structure in Sr_2RhO_4 evolves around T_S, and it can influence the nonequilibrium dynamics of photo-induced carriers as well as realtime phonon responses.

DOI: 10.1103/PhysRevB.100.235139

The interactions between charge, spin, orbital, and lattice degrees of freedom are crucial to determine quantum phases in correlated electron systems. $Ca_{2-x}Sr_xRuO_4$ is a representative example to investigate how the lattice structure governs the ground states ranging from an unconventional superconductor Sr_2RuO_4 [1] to a Mott insulator Ca_2RuO_4 [2]. Sr_2RuO_4 presents a quasi-two-dimensional layer composed of RuO_6 octahedra without any distortions in bulk [1]. Cation substitution with Ca^{2+} ions induces tilting and rotational distortions of the octahedra, which results in Mott gap opening as well as spin/orbital orderings [3,4]. In addition, Sr_2RuO_4 has a distinguished surface state originating from the topmost monolayer with rotational distortions, which hybridize d orbitals and produce an exceptional ferromagnetic order [5]. It shows that structural deformation especially in the octahedral structure is critical to modify the ground states of correlated materials based on the perovskite structure.

Layered perovskites Sr_2RhO_4 and Sr_2IrO_4, along with the ruthenates, have offered an opportunity to study the effects of octahedral distortions. Octahedral rotations about the c axis by $\sim 10°$ in Sr_2RhO_4 and Sr_2IrO_4 [6] turn their ground states into a clean correlated metallic phase [7] and an antiferromagnetic insulating phase [8], respectively. Intense studies have revealed that Sr_2IrO_4 is a spin-orbit coupled $J_{\text{eff}} = 1/2$ magnet, but the magnetic ground state of Sr_2RhO_4 is still unknown despite being isostructural with the layered iridate, except for a report on a two-dimensional short-range antiferromagnetic order [6,9]. Moreover, Sr_2RhO_4 has rarely been investigated in regard to its temperature (T) dependence of the octahedral structures, except for a neutron scattering result [10].

Here, we performed optical pump-probe experiments on Sr_2RhO_4 to investigate nonequilibrium dynamics of photoinduced carriers. In time-resolved reflectivity data, we found two different T-dependent anomalies. We observed that the ultrafast dynamics of photoinduced reflectivity slows down below $T_S \sim 160$ K. In addition, Sr_2RhO_4 shows T-dependent variations in coherent oscillations of the A_{1g} symmetry phonon, which corresponds to RuO_6 octahedral rotations in the quasi-two-dimensional plane. The coherent A_{1g} phonon presents clear anomalies across T_S of a huge change in its oscillation phase by 90° and a redshift in frequency below T_S. The unexpected feature in the coherent phonon of Sr_2RhO_4 suggests structural deformation in the octahedral rotations.

We utilized femtosecond near-infrared pulses to trace real-time reflectivity change upon photoexcitations in Sr_2RhO_4. Time-resolved reflectivity was measured with 800-nm pulses of pump and probe beams from a commercial Ti:sapphire amplifier system at a 250-kHz repetition rate. The full width at half maximum of the spot sizes were set to be 100 and 60 μm for the pump and probe beams, and we used pump fluences ranging from 20 to 4000 $\mu J\,cm^{-2}$ and probe fluence of 30 $\mu J\,cm^{-2}$. The time duration of pump and probe pulses is 30 fs. To minimize pump scattering noise, we used light polarizations of pump and probe beams perpendicular to each other. We performed first-principle calculations based on density functional theory (DFT) by using the PBEsol exchange correlation functional as implemented in the Vienna *ab initio* Simulation Package [11,12]. We used an $8 \times 8 \times 4$ k-point mesh and a kinetic energy cutoff value of 500 eV. The Hellman-Feynman forces are converged to 0.5 meV/Å for the structural relaxation, and we used the frozen phonon method to calculate the zone-center phonon modes.

*Corresponding author: mclee@lanl.gov; Present address: Center for Integrated Nanotechnologies, Los Alamos National Laboratory, Los Alamos, New Mexico 87545, USA.

†Corresponding author: kyungwan.kim@gmail.com

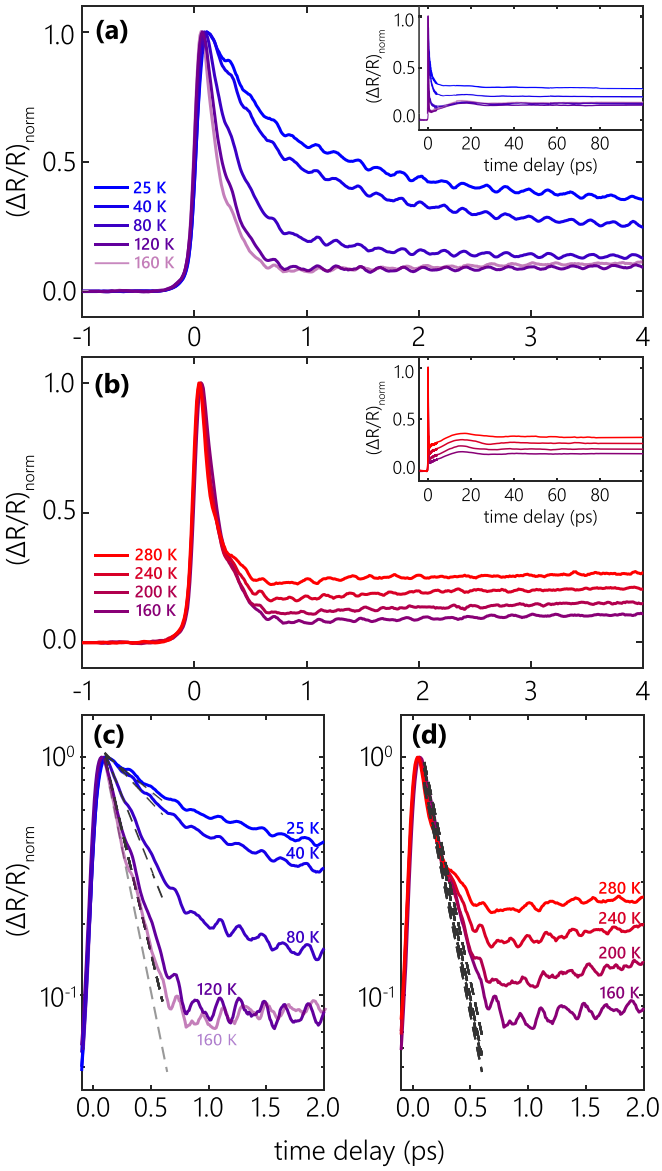

FIG. 1. Temperature dependent reflectivity changes in Sr_2RhO_4 stimulated by near-infrared optical pulses (a) from 25 to 160 K and (b) from 160 to 280 K. The data $(\Delta R/R)_{norm}$ were normalized by the maximum peak values. The same data are presented on a logarithmic scale in (c) and (d). The dashed lines are linear fits to verify the scattering rate of the initial exponential decay.

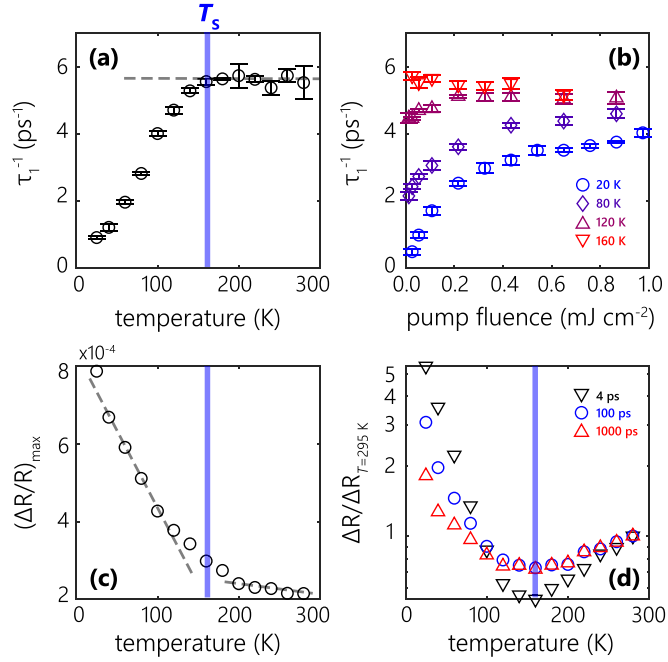

FIG. 2. Fitting parameters of scattering rate as a function of (a) temperature and (b) pump fluence. Reflectivity change at (c) maximum peak and (d) a few time points, $t = 4$, 100, 1000 ps. The data of each time point in (d) are normalized by the value at $T = 280$ K.

Figure 1 shows T-dependent time-resolved reflectivity from 25 to 280 K measured under pump fluence of 85 μJ cm^{-2}. The data $(\Delta R/R)_{norm}$ were normalized by their maximum peak values. The decaying transient of the photoinduced reflectivity is composed of two parts: (1) a relaxation component and (2) coherent oscillations. Scattering among the hot photoinduced carriers after pumping gives rise to the initial maximum change [13,14]. Thereafter, the energy of the hot carriers dissipates into other subsystems such as phonons, showing exponential relaxation dynamics. On the top of the overall dynamics, periodic oscillations are observed as shown in Fig. 1. The faster oscillation components with periods of a few hundred femtoseconds are driven by optical phonons [15], while the slower one with a 15-ps period is generated by a strain wave propagating along the c axis [16].

Sr_2RhO_4 shows clear T-dependent variations in its photoinduced reflectivity. Upon cooling, relaxation dynamics becomes slower in low temperatures, as shown in Figs. 1(a) and 1(b). Logarithmic plots in Figs. 1(c) and 1(d) present the T dependencemore clearly: The initial relaxation at $t <$ 0.25 ps is almost identical above 160 K, while it gradually slows down below 160 K. To articulate the T dependence, we fitted the reflectivity change on a logarithmic scale to a linear function [17]. We only used the data for $t < 0.25$ ps to extract a scattering rate of the initial exponential decay and to ignore other contributions from acoustic phonon oscillations or a long-lived component. The fitting results are displayed as dashed lines in Figs. 1(c) and 1(d).

In Figs. 2(a) and 2(b) we plot the fitting results of scattering rate $\gamma = 1/\tau$, where τ is the time constant of the initial decay. Figure 2(a) shows the T-dependent scattering rate. We find a huge suppression in γ at low temperatures, where the T-dependent anomaly starts to occur at around $T_S \sim 160$ K as temperature decreases. Figure 2(b) displays γ as a function of pump fluence. It is obvious that the scattering rate increases as optical pumping gets stronger only at low temperatures, below 160 K. The fluence dependence at low temperature might partly be explained by the pump-induced heating effect. However, the saturation characteristics of the fluence dependence at different temperatures cannot be explained only by the heating. We note that the fluence dependent changes of the scattering rate at different temperatures cannot be matched to each other by adjusting the fluence to account for such a heating effect. Therefore, the T- and fluence-dependent

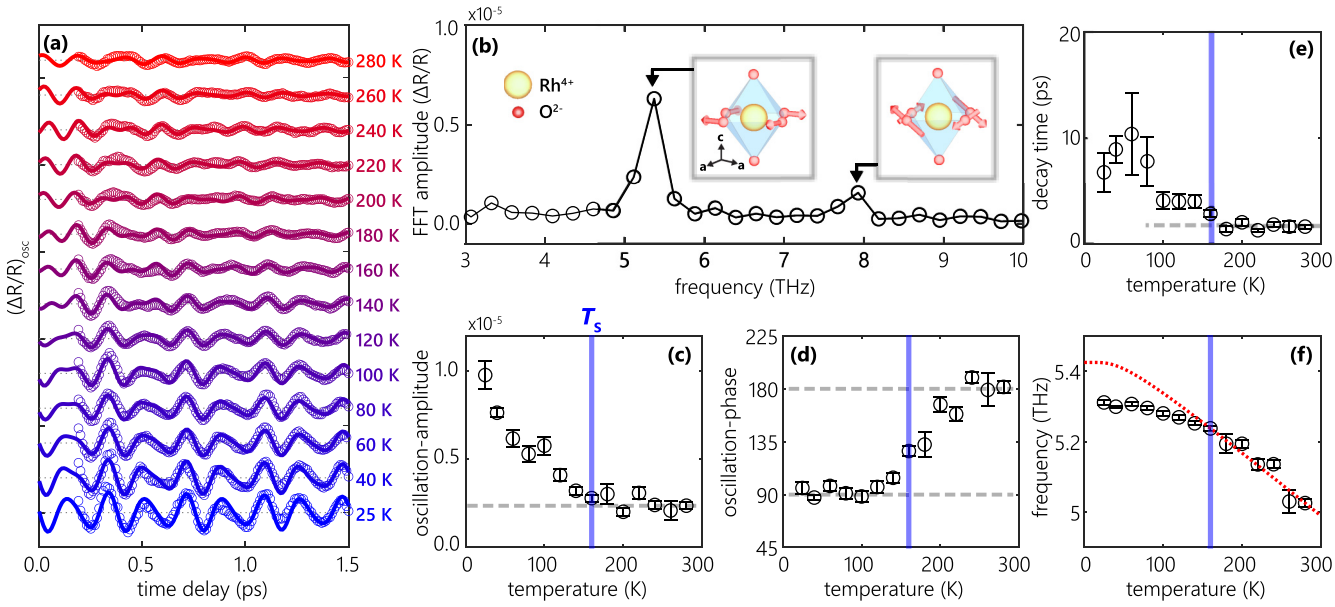

FIG. 3. (a) Coherent oscillations of photoinduced reflectivity change measured at various temperatures from 25 to 280 K. We extracted the coherent phonon oscillations by means of biexponential decay fits to the raw data of $\Delta R/R$. (b) Fourier transform of the coherent oscillations in (a). Two resonant oscillations correspond to the A_{1g} Raman phonons. (c)–(e) Fitting parameters of the coherent oscillations from the lower frequency A_{1g} symmetry phonon. The data are obtained by using a damped harmonic oscillator model. (f) The oscillation component of the lower frequency phonon after subtracting the higher frequency mode oscillations from (a). All error bars resulted from the model fitting of Eq. (1).

anomalies clearly indicate a characteristic change in physical properties of Sr_2RhO_4 across 160 K.

The increase of the scattering rate by intense optical pumping has been observed in correlated materials with an electronic gap. For instance, Sr_2IrO_4 exhibits a similar feature in its scattering rate due to a gap opening below the Néel temperature [18]. Once a gap opens at the Fermi level, the electron relaxation dynamics gets slower because the scattering with low energy phonons cannot contribute to the relaxation across the gap. Instead, the recombination of electron-hole pairs governs the relaxation dynamics across the gap, which shows a bimolecular behavior of faster dynamics at higher fluence [19–22]. Interestingly, a gap of 10 meV has been reported in Sr_2RhO_4 at low temperature due to rotational distortions [23]. However, the gap is not at the Fermi level but below the Fermi level, and Sr_2RhO_4 stays metallic in our temperature window [7,23]. Such a gap may influence the relaxation but the dynamics should be governed only by the relaxation process of the hole instead of the bimolecular electron-hole recombination. It is not clear yet whether the reported gap should show any characteristic change at T_S, and a further temperature dependent study of the gap and its relation to the relaxation dynamics is desired - e.g., time- and angle-resolved photoemission spectroscopy [24].

The raw data of the reflectivity transients present additional features in the T-dependent evolution across T_S. In Fig. 2(c), we plot the maximum peak of reflectivity change as a function of temperature. We observed that the peak value shows two different temperature regions with distinct linear T dependences below and above T_S. This can be due to the development of slow relaxation below T_S, as suggested by the decrease of the scattering rate γ. However, the data do not show a sharp anomaly at T_S but a gradual change in the slope from 120 to 200 K, suggesting that the T-dependent evolution can arise in a wide range of temperatures. Figure 2(d) shows reflectivity changes $\Delta R/R$ at $t = 4$, 100, and 1000 ps. The data are normalized by the data at 280 K for clear comparison of the T dependence. We found that all of the data present the minima at $T = 160$ K and distinct T dependences below and above T_S as found by $(\Delta R/R)_{max}$. The anomaly in the reflectivity change around T_S found over the whole time window suggests that there should be a corresponding change in the electronic and/or lattice structures across T_S.

We found additional evidence of the distinct evolution across T_S in the coherent phonon oscillations: Periodic modulations in optical probing signals driven by Raman active phonons after photoexcitations with femtosecond pulses [15,16,25–32]. The real-time phonon observation has offered another scope for crystal structures. Recently, ultrafast spectroscopic studies on Ca_2RuO_4 revealed that lattice deformation can induce anomalous changes in oscillation phases [25,26]. These studies on coherent phonons provided a new approach to investigate octahedral structures in correlated systems.

Figure 3(a) displays the oscillation components due to optical phonons $(\Delta R/R)_{osc}$ (open circles), which were extracted from the raw reflectivity transients after subtracting the electronic relaxation part based on the bi-exponential decay model [33]. Figure 3(b) shows the Fourier transform of the oscillating data, and two resonant modes correspond well to the A_{1g} symmetry Raman phonons as confirmed by our DFT calculations. While the eigenmode of the 5.3 THz A_{1g}

phonon is solely composed of the octahedral rotations of the in-plane oxygen, the vibrations along the c axis are added in the 7.8 THz mode, as shown in the inset of Fig. 3(b).

With the values of the resonant frequencies from the Fourier transform, we fit the data by means of a damped harmonic oscillator model:

$$(\Delta R/R)_{\rm osc}(t) = -\Sigma_i C_i \cos(2\pi f_i + \phi_i)\exp(t/\tau_i), \quad (1)$$

where C_i, f_i, ϕ_i, and τ_i present the amplitude, frequency, initial phase, and damping time of the A_{1g} symmetry phonons. We plot the fitting results as solid line curves in Fig. 3(a), which match the experimental data well. Figures 3(c)–3(e) show the fitting parameters of the oscillation amplitude, phase, and decay time of the 5.3 THz mode, which is the major component of the coherent oscillations, as shown in Fig. 3(b). The fitting parameters show a clear anomaly of a large shift in the phase across T_S [Fig. 3(d)] as well as an increase of the amplitude below T_S [Fig. 3(c)]. The decay time of the 5.3 THz phonon shows an apparent increase below T_S [Fig. 3(e)] while the oscillation frequency gradually increases as temperature decreases [Fig. 3(f)].

The 90° shift in the oscillation phase of coherent phonons is unusual in an absorbing medium. Once a material absorbs light, the equilibrium coordinate of the lattice can be shifted due to a change in the charge density distribution [15]. In other words, the equilibrium position in the photoexcited state ($Q_0^{\rm ex}$) should be shifted from that in the ground state (Q_0) (see Fig. 1 in Ref. [26]). This discrepancy in the equilibrium locations drives the displacive type force to the lattice generating coherent phonon oscillations with a cosine-type motion. The displacive motions in the lattice arise as periodic modulation in optical probing signals such as reflectivity with $\Delta R_{\rm osc} = (\partial R/\partial Q)\Delta Q$. Because Sr_2RhO_4 absorbs light with 1.55 eV of the energy of our pumping light at all temperatures (not shown), coherent phonon oscillations were expected to be of displacive cosine type. However, the 5.3-THz phonon turns into sine-type oscillations below T_S, which has been rarely observed in opaque materials except in the antiferromagnet Ca_2RuO_4 [26].

The abnormal phase shift even in the resonant condition can be attributed to a structural modulation along the phonon coordinate. As in the case of Ca_2RuO_4, a gradual distortion in the ground state towards the phonon coordinate ΔQ_{ph} can reduce the amplitude of displacive-type oscillations $\Delta R_{\rm osc}$ as $\Delta Q = Q_0^{\rm ex} - Q_0$ becomes zero [25,26]. Specifically, as the octahedral structure distorts upon cooling, the A_{1g} phonon oscillations may turn into sine-type vibrations induced by impulsive stimulated Raman scattering processes [27,28], which are usually screened out by the displacive mechanism in an opaque material [28,34]. The 90°-phase shift of the A_{1g} phonon oscillations in Ca_2RuO_4 can be driven by lattice deformation of octahedral tilting distortions with the antiferromagnetic spin ordering [26].

Accordingly, we argue that structural modulation along the A_{1g} phonon coordinate in Sr_2RhO_4 can change the generation mechanism of the coherent phonon. We also found evidence of the lattice deformation from the previous neutron scattering result [10]. As shown in Fig. S2 of the Supplemental Material [33], the T-dependent rotation angle of RuO_6 indicates a change in the trend of thermal evolution of the octahedral structure across $T \sim T_S$. Additionally, one can notice that the phase shift proceeds from 120 to 200 K, suggesting a wide T range of the structural evolution, consistent with the maximum values of reflectivity transient [Fig. 2(c)].

Nevertheless, the stronger phonon oscillation below T_S demands an explanation. The structural distortions in the octahedral rotations may account for the suppression in the displacive-type oscillations, but not the larger amplitude of the impulsive-type ones. The strength of the impulsive phonons should be subdued as $\delta Q = Q_0^{\rm ex} - Q_0$ becomes zero without any other contribution to the phonon. We found a feature of the interaction with the phonon in the T dependence of oscillation frequency, as shown in Fig. 3(f). In general, a gradual redshift as temperature increases originates from the anharmonic effects by phonon-phonon scattering with a model of $\omega(T) = \omega_0 - C[1 + 2/(e^{(\hbar\omega_0/kT)} - 1)]$, where $\omega(T)$ is a T-dependent phonon frequency and ω_0 is the frequency at zero temperature [35]. However, the anharmonic model does not fit with the frequency of the 5.3-THz phonon below T_S, while the model almost perfectly explains the 7.8-THz data (Fig. S3) [33]. The result indicates an extra interaction with the phonon, inducing a redshift below T_S.

As in Sr_2RhO_4, Ca_2RuO_4 presents a redshift in the phonon frequency of the A_{1g} mode with stronger impulsive amplitudes in the magnetic phase. The spin-phonon coupling leads to the softening in the phonon frequency in Ca_2RuO_4 [26] as in the cases of correlated magnetic materials [36,37]. In addition, it was suggested that the spin-phonon interaction can enhance the phonon amplitude of Ca_2RuO_4 [26]. The phonon anomalies of Sr_2RhO_4 could also be induced by a short-range antiferromagnetic order, suggested based on the result that magnetic susceptibility presents a peak at 200 K [6,9]. However, we cannot rule out other possibilities of electron-phonon or phonon-phonon interactions for the anomalous behaviors of the Sr_2RhO_4 phonon.

In summary, we investigated nonequilibrium dynamics of photoinduced carriers in Sr_2RhO_4 by using optical pump-probe spectroscopy. The relaxation dynamics after optical photoexcitations present clear T-dependent anomalies across $T_S \sim 160$ K. The coherent A_{1g} phonon oscillation changes from sine-type oscillations to smaller cosine-type oscillations as temperature increases across T_S. We suggest that the unexpected variation in the A_{1g} phonon oscillations as well as in the relaxation dynamics are driven by the structural deformation related to the octahedral rotations across T_S.

This work was supported by the Institute for Basic Science (IBS) in Korea (Grants No. IBS-R009-D1 and No. IBS-R009-G2). K.W.K. was supported by the Basic Science Research Program through the National Research Foundation of Korea (NRF) funded by the Ministry of Science, ICT and Future Planning (NRF-2017R1A4A1015323, 2018K1A3A1A21042482, and 2019R1F1A1062847).

[1] Y. Maeno, H. Hashimoto, K. Yoshida, S. Nishizaki, T. Fujita, J. G. Bednorz, and F. Lichtenberg, Nature (London) **372**, 532 (1994).

[2] S. Nakatsuji, S. Ikeda, and Y. Maeno, J. Phys. Soc. Jpn. **66**, 1868 (1997).

[3] S. Nakatsuji and Y. Maeno, Phys. Rev. Lett. **84**, 2666 (2000).

[4] I. Zegkinoglou, J. Strempfer, C. S. Nelson, J. P. Hill, J. Chakhalian, C. Bernhard, J. C. Lang, G. Srajer, H. Fukazawa, S. Nakatsuji, Y. Maeno, and B. Keimer, Phys. Rev. Lett. **95**, 136401 (2005).

[5] R. Matzdorf, Z. Fang, Ismail, J. Zhang, T. Kimura, Y. Tokura, K. Terakura, and E. W. Plummer, Science **289**, 746 (2000).

[6] M. A. Subramanian, M. K. Crawford, R. L. Harlow, T. Ami, J. A. Fernandez-Baca, Z. R. Wang, and D. C. Johnston, Physica C **235**, 743 (1994).

[7] R. S. Perry, F. Baumberger, L. Balicas, N. Kikugawa, N. J. C. Ingle, A. Rost, J. F. Mercure, Y. Maeno, Z. X. Shen, and A. P. Mackenzie, New J. Phys. **8**, 175 (2006).

[8] B. J. Kim, Hosub Jin, S. J. Moon, J.-Y. Kim, B.-G. Park, C. S. Leem, Jaejun Yu, T. W. Noh, C. Kim, S.-J. Oh, J.-H. Park, V. Durairaj, G. Cao, and E. Rotenberg, Phys. Rev. Lett. **101**, 076402 (2008).

[9] T. Shimura, M. Itoh, and T. Nakamura, J. Solid State Chem. **98**, 198 (1992).

[10] T. Vogt and D. J. Buttrey, J. Solid State Chem. **123**, 186 (1996).

[11] G. Kresse and J. Hafner, Phys. Rev. B **47**, 558 (1993).

[12] G. Kresse and D. Joubert, Phys. Rev. B **59**, 1758 (1999).

[13] R. D. Averitt and A. J. Taylor, J. Phys.: Condens. Matter **14**, R1357 (2002).

[14] C. Giannetti, M. Capone, D. Fausti, M. Fabrizio, F. Parmigiani, and D. Mihailovic, Adv. Phys. **65**, 58 (2016).

[15] H. J. Zeiger, J. Vidal, T. K. Cheng, E. P. Ippen, G. Dresselhaus, and M. S. Dresselhaus, Phys. Rev. B **45**, 768 (1992).

[16] C. Thomsen, J. Strait, Z. Vardeny, H. J. Maris, J. Tauc, and J. J. Hauser, Phys. Rev. Lett. **53**, 989 (1984).

[17] Considering photoinduced reflectivity change as a single exponential function $\Delta R/R(t) = A\exp(-\gamma t)$, the slope of a linear fitting on logarithmic data should correspond to the scattering rate of the exponential decay: $\ln(\Delta R/R) = -\gamma t + \ln(A)$.

[18] D. Hsieh, F. Mahmood, D. H. Torchinsky, G. Cao, and N. Gedik, Phys. Rev. B **86**, 035128 (2012).

[19] J. Demsar, B. Podobnik, V. V. Kabanov, T. Wolf, and D. Mihailovic, Phys. Rev. Lett. **82**, 4918 (1999).

[20] N. Gedik, P. Blake, R. C. Spitzer, J. Orenstein, Ruixing Liang, D. A. Bonn, and W. N. Hardy, Phys. Rev. B **70**, 014504 (2004).

[21] E. E. M. Chia, Jian-Xin Zhu, H. J. Lee, Namjung Hur, N. O. Moreno, E. D. Bauer, T. Durakiewicz, R. D. Averitt, J. L. Sarrao, and A. J. Taylor, Phys. Rev. B **74**, 140409(R) (2006).

[22] A. Rothwarf and B. N. Taylor, Phys. Rev. Lett. **19**, 27 (1967).

[23] F. Baumberger, N. J. C. Ingle, W. Meevasana, K. M. Shen, D. H. Lu, R. S. Perry, A. P. Mackenzie, Z. Hussain, D. J. Singh, and Z.-X. Shen, Phys. Rev. Lett. **96**, 246402 (2006).

[24] U. Bovensiepen and P. S. Kirchmann, Laser Photonics Rev. **6**, 589 (2012).

[25] M.-C. Lee, C. H. Kim, I. Kwak, J. Kim, S. Yoon, B. C. Park, B. Lee, F. Nakamura, C. Sow, Y. Maeno, T. W. Noh, and K. W. Kim, Phys. Rev. B **98**, 161115(R) (2018).

[26] M.-C. Lee, C. H. Kim, I. Kwak, C. W. Seo, C. Sohn, F. Nakamura, C. Sow, Y. Maeno, E.-A. Kim, T. W. Noh, and K. W. Kim, Phys. Rev. B **99**, 144306 (2019).

[27] L. Dhar, J. A. Rogers, and K. A. Nelson, Chem. Rev. **94**, 157 (1994).

[28] T. E. Stevens, J. Kuhl, and R. Merlin, Phys. Rev. B **65**, 144304 (2002).

[29] G. A. Garrett, T. F. Albrecht, J. F. Whitaker, and R. Merlin, Phys. Rev. Lett. **77**, 3661 (1996).

[30] J. J. Li, J. Chen, D. A. Reis, S. Fahy, and R. Merlin, Phys. Rev. Lett. **110**, 047401 (2013).

[31] D. M. Riffe and A. J. Sabbah, Phys. Rev. B **76**, 085207 (2007).

[32] A. V. Kuznetsov and C. J. Stanton, Phys. Rev. Lett. **73**, 3243 (1994).

[33] See Supplemental Materialat http://link.aps.org/supplemental/10.1103/PhysRevB.100.235139 for additional experimental details.

[34] J. Franck, Trans. Faraday Soc. **21**, 536 (1926).

[35] M. Balkanski, R. F. Wallis, and E. Haro, Phys. Rev. B **28**, 1928 (1983).

[36] C. H. Sohn, C. H. Kim, L. J. Sandilands, N. T. M. Hien, S. Y. Kim, H. J. Park, K. W. Kim, S. J. Moon, J. Yamaura, Z. Hiroi, and T. W. Noh, Phys. Rev. Lett. **118**, 117201 (2017).

[37] J. Son, B. C. Park, C. H. Kim, H. Cho, S. Y. Kim, L. J. Sandilands, C. H. Sohn, J.-G. Park, S. J. Moon, and T. W. Noh, npj Quantum Mater. **4**, 17 (2019).